Raman Spectroscopy and Confocal Raman Imaging

by
Mårten Pålsson

Master's Thesis
Lund Reports on Atomic Physics, LRAP-292
Lund, January 2003

Table of contents

1. Introduction

This thesis deals with the possible use of a laser scanning confocal microscope to conduct Raman imaging.

Raman spectroscopy is an optical technique for measuring the vibrational energies in molecules. With Raman spectroscopy it is possible to identify which molecules are present in a sample. Raman spectroscopy is just one of many optical spectroscopy techniques for studying samples. The major potential of Raman spectroscopy compared to other methods is the possibility of easily identifying many different compounds in the same sample. If you combine Raman spectroscopy with imaging techniques you get Raman imaging. With Raman imaging it is possible to obtain information about the spatial distribution of molecular species within a sample.

Due to the low cross section for Raman scattering, the Raman signals are extremely weak. This weakness results in that other scattering processes, such as fluorescence, may severely affect the possibility of performing Raman spectroscopy. To conduct Raman spectroscopy you therefore have to use methods to reduce fluorescence. One method is to use near-infra red excitation light, which has energy not high enough to cause fluorescence for most molecules.

The thesis begins with a theoretical overview of different scattering processes. In chapter three an overview of Raman spectroscopy and Raman Imaging is given. Chapter four deals with the theory of confocal microscopes and photomultiplier tubes which are used as detectors in confocal microscopes.

Initially Raman spectroscopy measurements were done to identify Raman peaks of various substances that could be used for Raman imaging. These measurements are described in chapter five.

Chapter seven describes the Raman microscopy measurements that were done to evaluate the performance of the laser scanning confocal microscope.

In chapter six finally the Raman imaging measurements are described.

2. Raman Theory

The objective of this chapter is to give an introduction to energy structures of molecules and the different scattering processes that may occur when light passes through a medium. In particular the theory of Raman scattering is described.

2.1 Molecular structure

A molecule consists of two or more atoms bond together. According to quantum mechanics the energy of an atom or a molecule is quantized into discrete energy states. In an atom these energy states correspond to different arrangements of its electrons. A molecule has additional energy states besides the electronic states. These energy states correspond to the vibrational and rotational motion of the molecule. The rotational motion of the molecule is defined as rotation around a principal axis and the vibrational motion of the molecule is a periodic change in the bond distances and/or the angles of the molecule. The total energy of a molecule is the sum of its electronic, vibrational and rotational energy. The energy levels of a molecule are schematically shown in Figure 2.1. The separation between the rotational energy states is in the order of 0.001 eV and between vibrational energy states in the order of 0.1 eV.

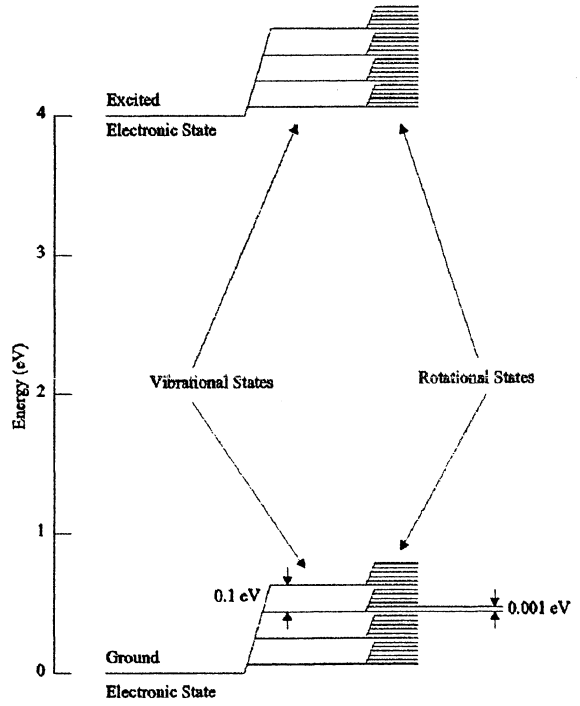

Figure 2.1 Schematic energy level diagram of a molecule. Modified from [1]

The vibration of a molecule is described by fundamental frequencies or modes corresponding to different types of vibrational motion. Each of these vibrational modes corresponds to a different vibrational energy level of the molecule.

An atom has three degrees of freedom, which corresponds to the three coordinates required to describe its position in space. A molecule consisting of N atoms thus has 3N degrees of freedom corresponding to the number of coordinates needed to describe the position of all of its atoms. To describe the position of the centre of gravity of the molecule takes three coordinates and to specify its orientation takes three coordinates. Thus, three degrees of freedom describe the translational motion of the molecule and three degrees of freedom describes the rotational motion of the molecule. This leaves 3N-6 degrees of freedom for the vibrational motion. In a linear molecule only 2 rotational degrees of freedom exists and thus there are 3N-5 degrees of freedom for vibrational motion. This is because in a linear molecule, such as H_2, rotation around the axis of the molecule results in no displacement of the nuclei and thus is not considered a degree of freedom. The vibrational degree of freedom for the molecule is the same as the number of normal modes of vibration for the molecule.

The normal vibrational modes in a molecule can be divided into stretching and bending modes. In stretching modes the distance between the atoms in the molecule changes and in bending modes the angle between the bonds changes. In Figure 1.2 some examples of different vibrational modes are shown.

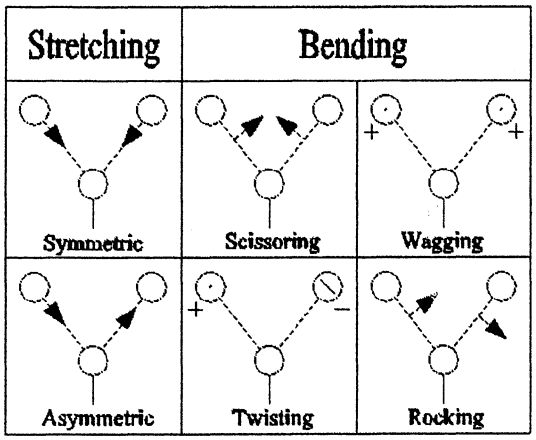

Figure 2.2 Vibrational modes of a molecule. The + and – signs signifies movement perpendicular to the plane of this page. Modified from [1].

2.2 Scattering Processes

When photons propagate trough a media they have a possibility of interacting with it. The photons might be absorbed or they might be scattered. These scatterings can be either elastic or inelastic.

When a photon is elastically scattered there is no net energy transfer between it and the media. The elastically scattered light keeps its original wavelength. When inelastic scattering occurs there is a net energy transfer between the photon and the media. The inelastically scattered light has a different wavelength than the incoming light.

2.2.1 Elastic scattering

Two types of elastic scattering is usually discussed, Mie and Rayleigh scattering. Their occurrence is dependent of the size of the scattering particle.

Mie scattering occurs when the wavelength of the light is much smaller than the scattering particle size. The probability of Mie scattering is dependent of the wavelength of the light, particle radius, index of refraction and absorption of the particle and the surrounding media. The function is complicated, but as a general rule the probability has approximately a λ^{-2} dependence, and therefore increases towards shorter wavelengths.

Rayleigh scattering occurs when the wavelength of the light is larger than the scattering particle size. The electric field of the light induces an electric dipole moment in the molecule. The molecule then reemits the light in a new direction. The probability of Rayleigh scattering has a λ^{-4} dependence, and therefore strongly increases towards shorter wavelengths.

The increased probability with shorter wavelengths for both Rayleigh and Mie scattering is the reason for the blue skies and the red sunsets. The probability of scattering is larger for blue light than for red light. When you look up at the sky you see the scattered blue light, but when you look towards the sunset you see the transmitted red light.

2.2.2 Inelastic scattering

If the energy of the photon is high enough it can excite a molecule to a higher electronic state by being absorbed. The molecule then almost instantaneously relaxes to the lowest level in the excited electronic state without emitting radiation. This process is caused by collision with other molecules and is called internal conversion. The molecule then deexcites down to the ground electronic state by emitting fluorescence light. The process is shown in Fig 2.3

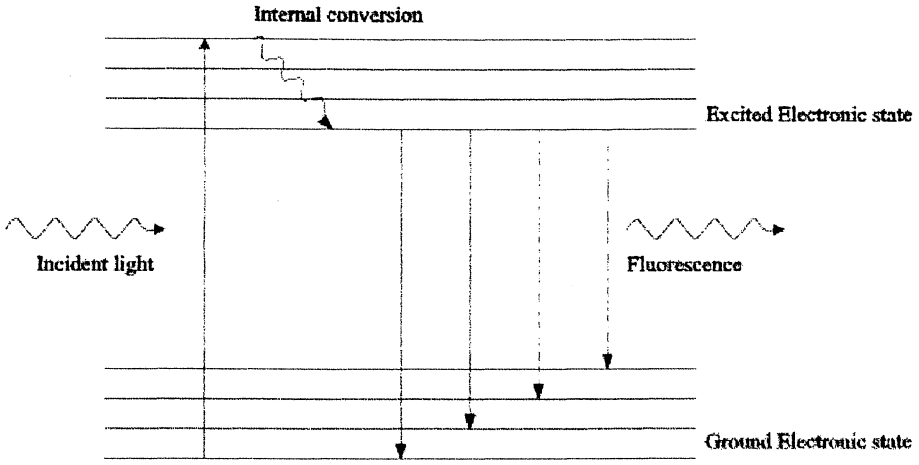

Figure 2.3 Fluorescence.

If the energy of the photons is not high enough to excite the molecule to a higher electronic state, Raman or Rayleigh scattering may occur. The molecule absorbs the photon and is excited up to a virtual level. The molecule then deexcites to one of the levels in the ground electronic state by emitting light. If the scattered photon has preserved its energy we have Rayleigh scattering. If the scattered photon has gained or lost energy we get Anti-Stokes and Stokes Raman scattering, respectively.

2.3 Raman scattering

Rayleigh and Raman scattering can be explained both classically and quantum mechanically.

2.3.1 Classical explanation of Raman scattering

Classically a molecule can be seen as a positively charged nucleus surrounded by a negatively charged cloud of electrons. When light interacts with a molecule the electric field of the electromagnetic wave can be approximated to be constant throughout the molecule. This is because the wavelength of light, which is in the order of 500 nm, is much larger when compared to the size of a molecule, which have a size in the order of 1 nm.

The electric field of the electromagnetic wave is given by

$$E = E_0 \cos(2\pi \nu_0 t) \tag{2.1}$$

Where E_0 is the amplitude of the electric field and ν_0 is the frequency of the electric field. The electric field E induces a dipole moment P in the molecule.

$$P = \alpha E = \alpha E_0 \cos(2\pi \nu_o t) \tag{2.2}$$

Where α is the polarizability of the molecule. Because of frequent asymmetry of molecules the induced dipole moment P is usually not parallel with the electric field E. The polarizabilty α must in this case be an tensor and not a scalar. With Cartesian coordinates the polarizability can be written as a matrix equation.

$$\begin{bmatrix} P_x \\ P_y \\ P_z \end{bmatrix} = \begin{bmatrix} \alpha_{xx} & \alpha_{xy} & \alpha_{xz} \\ \alpha_{yx} & \alpha_{yy} & \alpha_{yz} \\ \alpha_{zx} & \alpha_{zy} & \alpha_{zz} \end{bmatrix} \begin{bmatrix} E_x \\ E_y \\ E_z \end{bmatrix} \tag{2.3}$$

If the molecule vibrates the polarizability will be changed. By assuming the vibration to be simple harmonic one, the displacement q from the equlibrium position can be expressed as

$$q = q_0 \cos(2\pi \nu_{vib} t) \tag{2.4}$$

Where q_0 is the amplitude and ν_{vib} is the frequency of the vibration. The polarizability changes as the molecule vibrates. For small vibrations the polarizability can be expanded as a Taylor series into (higher order terms are neglected because of the small amplitude).

$$\alpha(q) = \alpha_0 + \left.\frac{\partial \alpha}{\partial q}\right|_{q_0} \cdot q + \ldots \tag{2.5}$$

Where α_0 is the polarizability and $\left.\frac{\partial\alpha}{\partial q}\right|_{q_0}$ is the derivative of the polarizability with respect to the vibration q at the equilibrium position q_0. Inserting (2.4) into (2.5) and then inserting the resulting expression for α into (2.2) yields

$$P = \alpha_0 E_0 \cos(2\pi\nu_0 t) + \left.\frac{\partial\alpha}{\partial q}\right|_{q_o} \cdot q_0 E_0 \cos(2\pi\nu_{vib} t)\cos(2\pi\nu_0 t) \qquad (2.6)$$

By using the trigonometric identity

$$\cos(\alpha)\cos(\beta) = \frac{1}{2}\left[\cos(\alpha+\beta) + \cos(\alpha-\beta)\right] \qquad (2.7)$$

Equation (2.6) can be rewritten as

$$P = \alpha_0 E_0 \cos(2\pi\nu_0 t) + \left.\frac{1}{2}\frac{\partial\alpha}{\partial q}\right|_{q_0} \cdot q_0 E_0\left[\cos(2\pi(\nu_0+\nu_{vib})t) + \cos(2\pi(\nu_0-\nu_{vib})t\right] \qquad (2.8)$$

This describes an oscillating dipole. The first term oscillates at ν_0 and produce elastic Rayleigh scattering, the second term oscillates at $\nu_0+\nu_{vib}$ and produces Anti-Stokes part of the Raman scattered light, the third term oscillates at $\nu_0-\nu_{vib}$ and produces Stokes part of the Raman scattered light.

For Raman scattering to occur $\left.\frac{\partial\alpha}{\partial q}\right|_{q_0} \neq 0$, which means that the polarizability α has to change with the displacement. A vibration mode in which this occurs is said to be Raman active. The value of the derivative is different for different molecules and some molecules will be strong Raman scatterers and other (like H_20) will not show any, or very weak, Raman scattering.

The intensity radiated from an oscillating dipole is proportional to the second time derivative of the induced dipole moment.

$$I \propto \left(\frac{\partial^2 P}{\partial t^2}\right)^2 \qquad (2.9)$$

Inserting equation (2.8) into this equation results in the following expressions for the intensity of the scattered light

$$I_{Rayleigh} \propto \nu_0^4 \alpha_o^4 I_0 \qquad (2.10)$$

$$I_{Stokes} \propto (\nu_0 - \nu_{vib})^4 \left(\left.\frac{\partial\alpha}{\partial q}\right|_{q=0}\right)^2 I_0 \qquad (2.11)$$

$$I_{Anti-Stokes} \propto (\nu_0 + \nu_{vib})^4 \left(\frac{\partial \alpha}{\partial q}\bigg|_{q=0} \right)^2 I_0 \qquad (2.12)$$

where I_0 is the intensity of incident light. As these equations show a strong frequency dependence of the scattering frequency ($I_{scattered} \propto \nu^4$).

Classical theory of Raman scattering predicts that the intensity of the Stokes and Anti-Stokes Raman scattering to be almost the same. This prediction is not true as experimental measurements shows that the Anti-Stoke scattering is much weaker than Stokes scattering. A quantum mechanical approach to Raman scattering can explain the difference in intensity between Stokes and Anti-Stokes Raman scattering.

2.3.2 Quantum mechanical approach to Raman scattering

The incident photon perturbs the molecular system and excites it up from the initial energy state to a virtual state. A virtual state is not an actual energy state as it do not correspond to any possible rotational, vibrational or electronic modes and therefore is a forbidden state according to quantum mechanics. From this virtual state the molecular system instantaneously relaxes down to any of the states in ground state by emitting a photon.

If the initial and final state are the same, the initial and the scattered photon will have the same energy and Rayleigh scattering has occurred. If the molecule relaxes to a higher state than the initial, the molecule has gained energy and the emitted photon has been Stokes shifted. If it relaxes to a lower state than the initial the molecule has lost energy, and the scattered photon has been anti-Stokes shifted.

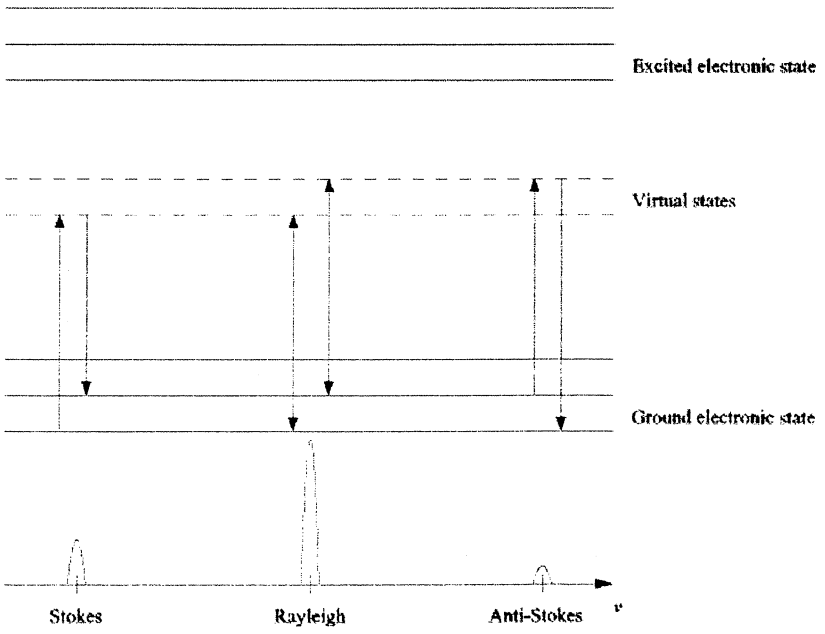

Figure 2.4 Rayleigh and Raman Scattering

The population of the vibrational energy state follows the Boltzmann distribution.

At normal temperatures almost all of the molecules are in their lowest vibrational state. Boltzmanns law gives the relation in population between two levels separated by an energy ΔE.

$$\frac{N_{lower}}{N_{upper}} = e^{\frac{\Delta E}{kT}} \tag{2.13}$$

where N is the population of the energy state, T is the absolute temperature in Kelvin and k is Boltzmann´s constant.

The ratio between Stokes and anti-Stokes Raman scattering, according to (2.11) and (2.12) , is modified with Boltzmann´s law

$$\frac{I_{Stokes}}{I_{anti-Stokes}} = \frac{\left(\nu_0 - \nu_{vib}\right)^4}{\left(\nu_0 + \nu_{vib}\right)^4} e^{\frac{\Delta E}{kT}} \tag{2.14}$$

At normal temperatures the ratio is very large and thus is the anti-Stokes Raman scattering very weak compared to the Stokes Raman scattering. At higher temperature the ratio decreases and the anti-Stokes Raman scattering grows stronger.

3. Raman spectroscopy

3.1 Introduction

Raman spectroscopy is an optical technique for measuring the vibrational energies in molecules. By using the Raman spectra it is possible to identify which chemical bonds that are present in a sample, and from this draw the conclusion which molecules are present. The major problem when conducting Raman spectroscopy is the very low intensity of the Raman scattered light, which is due to the low probability of Raman scattering. As a result of this other scattering effects, such as fluorescence, will show a higher intensity and severely affect the possibility of measuring the Raman signals.

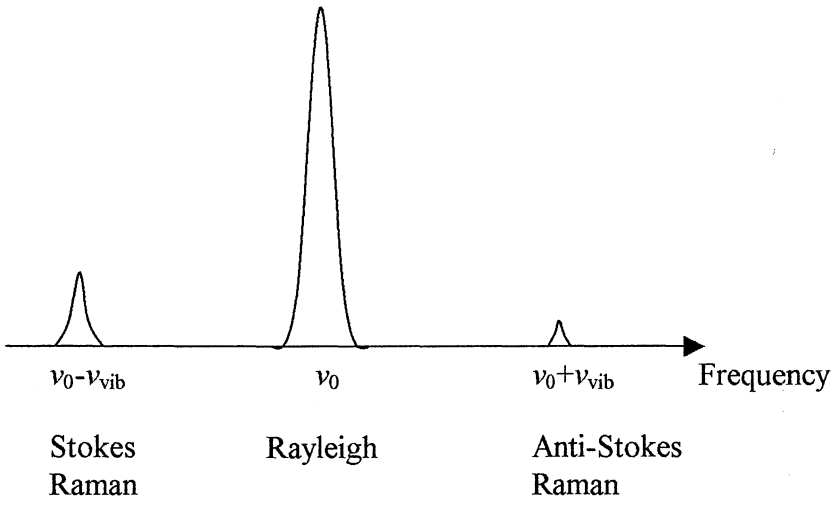

Figure 3.1 Raman spectra with one molecular vibration.

A schematic Raman spectra is shown in Figure 3.1. When performing Raman spectroscopy, you identify the light with the frequency shift from excitation light. The reason for this is that frequency shift for a Raman peak is independent of the wavelength of the excitation light. As the frequency shifts are in the order of 10^{-12} s^{-1}, the frequency is usually divided by the speed of light. The resulting quantity is then a wavenumber, which is defined by

$$\Delta\bar{\nu} = \frac{\nu}{c} = \frac{1}{\lambda} \tag{3.1}$$

Where ν is the frequency, c is the speed of light and λ is the wavelength. The usually used unit of $\Delta\bar{\nu}$ is cm^{-1}.

At zero frequency shift is the Rayleigh line, which is the elastically scattered excitation light. On either side of the Rayleigh line are the Raman peaks of the Stokes and Anti-Stokes Raman scattering. The absolute frequency shifts of peaks coming from one molecular vibration are equal.

3.2 Fluorescence reduction

Fluorescence background is a major problem when performing Raman spectroscopy. The low cross section of Raman scattering compared to fluorescence is the cause of this. Relative to the Raman signal the fluorescence background can be up to 10^8 times stronger.

A number of different methods can be used to reduce the fluorescence in the spectra when conducting Raman spectroscopy. These methods all take advantage of the differences between Raman scattering and fluorescence. The major differences are

- Fluorescence, opposed to Raman scattering, only occurs if the molecule is excited up to a higher electronic state.
- Fluorescence has a longer lifetime than Raman scattering.
- Fluorescence emission is broadband while Raman peaks are narrow.
- Fluorescence is unpolarized while Raman scattering can be polarized.
- Fluorescence emission occurs only at longer wavelengths than the excitation source.

The methods taking advantage of these differences to reduce the fluorescence can either be experimental or mathematical. The mathematical methods are used on the data from the measurements, while the experimental ones is implemented in the experimental set-up.

A brief introduction to some of the different methods is found below.

Experimental

Near-infrared excitation. Selection of an optimal excitation wavelength is an effective way to suppress fluorescence. By using a longer wavelength, the energy of the photons is not high enough to excite the molecules to their first electronic state and cause fluorescence. By choosing excitation light in the near-infrared region, a major part of the fluorescence background is eliminated for most compounds. This method has some drawbacks as the cross section for Raman scattering is reduced with an increasing wavelength at λ^{-4}. The sensitivity of detectors is also reduced at longer wavelengths

Temporal gating. The lifetime for Raman scattering is ~10^{-12}s and fluorescence ~10^{-9}s. By using a pulsed laser and a time-gated signal detection, so that only the early photons is detected, the short lived Raman signal scattering is detected and long lived fluorescence emission is rejected. A disadvantage with the method is that the high intensity of a short laser pulse may damage the sample. The application of this method to suppress fluorescence is shown in reference [2]

Anti-Stokes Raman spectroscopy. By using the Anti-Stokes Raman lines there is no fluorescence. At room temperature the Anti-Stokes Raman signals are so weak that it is impossible to detect them. This method can be used in combustion process at higher temperatures [3].

Mathematical methods

Polynomial fit. By fitting a polynomial of an order high enough to describe the slow varying fluorescence spectra, but not the sharp Raman peaks. Subtracting this polynomial from the spectra will remove or at least reduce the influence of fluorescence and yield only the Raman peaks.

Fast Fourier Transform. This procedure is similar to the polynomial fit, with the difference that the discrimination is done in the frequency domain. The spectra is Fourier transformed, and the broad features such as fluorescence will appear as low spatial frequencies compared to the sharp Raman peaks which will yield higher spatial frequencies. A highpass filter is applied and an inverse fast fourier transform is done to obtain the spectra without fluorescence.

3.3 Raman Imaging

Raman imaging, which combines Raman spectroscopy and imaging techniques, is an excellent method for obtaining information about the spatial distribution of molecular species. For example, Raman imaging has been used to map the distribution of cholesterol in the lens of a rat eye [4].

The principle on which Raman Imaging is based, is that the spatial distribution of a molecular species is obtained by isolating the Raman scattered photons from a Raman line of the specific molecular species. Raman imaging is not a simple method because of the weak Raman signals, due to the low probability of Raman scattering.

Raman Imaging methods can be divided into two different categories, direct-imaging and series-imaging techniques. The difference between the two is how they deal with the fact that Raman Imaging is a 3-dimensional problem (1 spectral and 2 spatial dimensions) while the maximal dimensions of detectors are 2.

Direct-imaging methods results in an immediate image of the spatial distribution of a compound within the sample. In direct-imaging methods the entire sample is illuminated at the same time (global sample illumination). The scattered radiation from the sample is collected and the desired Raman line is spectrally filtered out before being received by a 2D detector. Raman direct-imaging is demonstrated in [5].

In series-imaging methods the sample is scanned and the image is reconstructed afterwards. Although you can use both single-element detectors and two-dimensional detectors for series imaging, the best results are obtained with two-dimensional detectors, such as a CCD [6]. Different examples of Raman series-imaging is demonstrated in [7, 8, 9]. There are two different types of series-imaging methods, point and line illumination.

In point illumination techniques a laser spot is scanned across the sample. At each resolved position the light is collected, spectrally filtered and detected by a detector. The major disadvantage with this method is that it is very-time consuming, as you have to collect data from many points to be able to reconstruct a image.

In line illumination techniques you reduce the data collection time by illuminating the sample along a line and detecting with a two dimensional-detector.

3.4 Signal-to-noise ratio considerations

Signals when conducting Raman spectroscopy can be very weak. Noise is a major problem because of the weak signals. The quality of a measurement can be expressed by the signal-to-noise ratio (S/N). The higher the signal-to-noise ratio, the more reliable the measurement. The weakest detectable signal is when the signal to noise ratio is one. The weakest detectable signal is called the noise equivalent power (NEP).

$$S = NEP \Leftrightarrow \frac{S}{N} = 1 \tag{3.2}$$

The most important source of noise is shot noise. Shot-noise arise from that the signals are quantized, and shows a statistical variation which obeys a Poisson distribution. If we have a signal that contains n particles the shot noise is equal to:

$$noise_{shot} = \sqrt{n} \tag{3.3}$$

Shot noise not only arises from the signal, but also from dark current in the detector. The total shot noise is given by

$$noise_{total} = \sqrt{noise_{signal}^2 + noise_{darkcurrent}^2} \tag{3.4}$$

If shot noise from the signal and the dark current in the detector are the only sources of noise in a measurement the signal to noise ratio is given by.

$$\frac{S}{N} = \frac{S}{\sqrt{noise_{signal}^2 + noise_{darkcurrent}^2}} \tag{3.5}$$

The signal-to-noise ratio above only takes into account the shot noise from the detector. When performing spectroscopy we have many other sources of noise, such as detector readout noise.

4. Theory of equipment used for Raman Imaging

The MRC 1024 (Bio-Rad Microscopy Division), which is used in the Raman Imaging measurements, is a laser scanning confocal microscope. In this chapter the theory of confocal microscopy and of photomultiplier tubes, which are used in the microscope, is presented.

4.1 Confocal Microscopy

The first confocal microscope was constructed and patented by Minksy in 1957 [6]. Confocal means "having the same focus".

Unlike a normal microscope, where the whole sample is illuminated, the confocal microscope only measures the light from a small volume in the sample at any one time. The principle of a confocal microscope is shown I Figure 4.1.

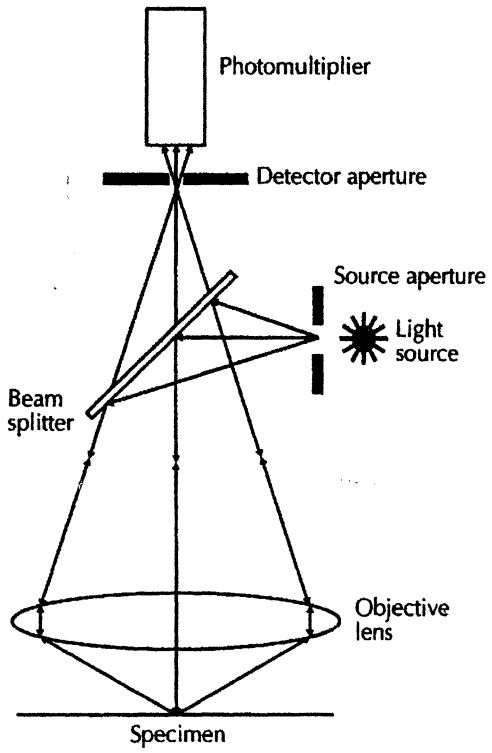

Figure 4.1 A schematic diagram of the principle utilized in a confocal microscope. [From 10]

The excitation light is focused on specimen by the objective lens. The scattered light from the specimen is collected by the same objective lens and focused onto a pinhole aperture. Only the scattered light from the focus is focused on pinhole and passes to the detector. Light from out-of-focus is not focused on the pinhole and will therefore be blocked from reaching the detector. The rejection of out-of-focus planes makes resolution in depth possible.

As the detector only sees one point of the specimen at one time it is necessary to move the illuminated point across the specimen to get an image. This can be done either by scanning the illuminated point (beam scanning) or by moving the specimen (stage scanning). Opposed to a conventional microscope, a confocal microscope needs some form of image processing to produce an image.

Instead of using a pinhole, it is possible to use infinity optics, see figure 4.2. The pinhole aperture in confocal imaging system must be small to get a good resolution. The use of a small aperture may pose serious problems of alignment. By using infinity optics, i.e. parallel rather than focused beams, the in-focus light returns as a parallel beam, and the out-of-focus light returns as a convergent or divergent beam. This allows the use of an iris diaphragm as aperture, which can be in the order of millimetres in size and is easily aligned.

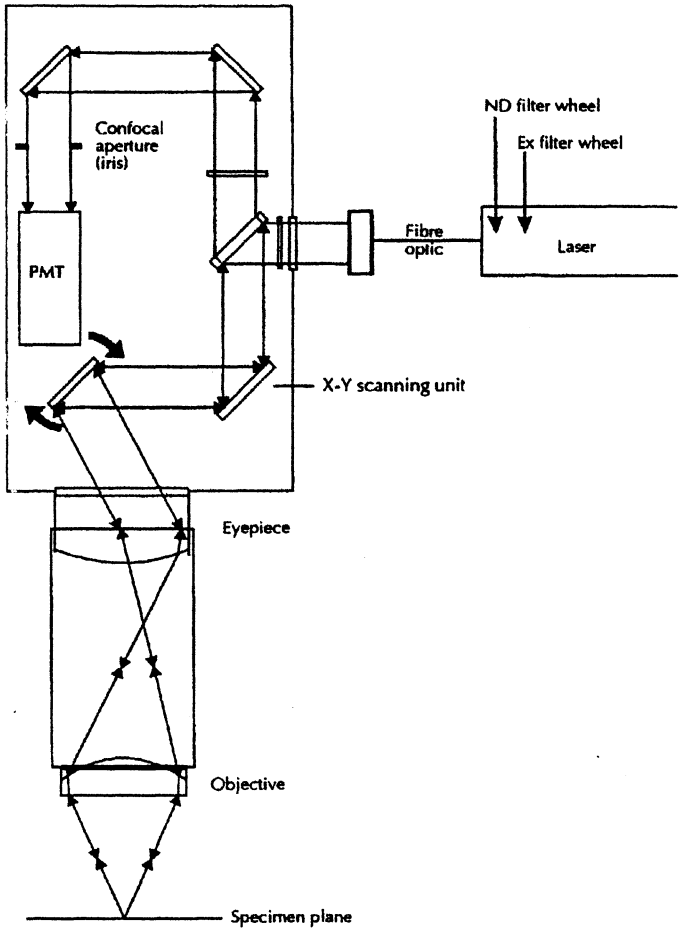

Figure 4.2 Schematic picture of a confocal infinity optics system [From 10]

4.1.1 Resolution

The limit of resolution is the smallest separation between two point objects while still allowing them to be resolved. The lateral resolution is measured perpendicular to the optical axis, and the axial resolution is measured along the optical axis.

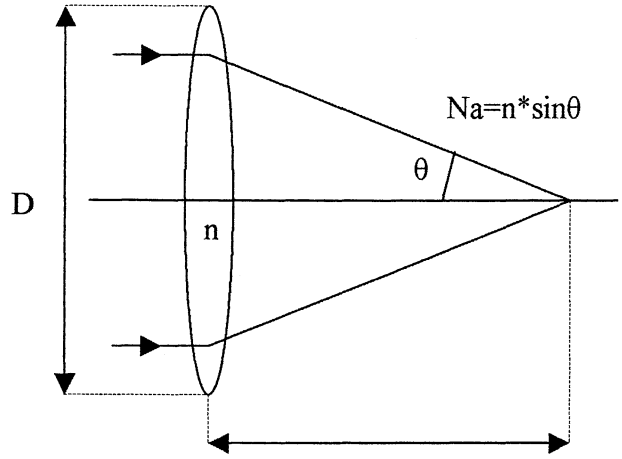

Figure 4.3 Microscope objective focusing and the definition of NA.

According to the Rayleigh criteria, two point objects are resolved when the principal maximum of the diffraction pattern for one point lies on the first minimum of the diffraction pattern for the other. For a point object the distance from the centre to the first minimum is defined as the Airy disk radius. The airy disk radius is given by:

$$r_{AIRY} = \frac{1.22\lambda}{2NA} \tag{4.1}$$

where λ is the wavelength and NA is the numerical aperture of the lens. The numerical aperture is given by:

$$NA = n\sin\theta \tag{4.2}$$

where θ is the angle and n the index of refraction .

The lateral resolution of a microscope also depends of the field of view. As the confocal pinhole size is decreased the field of view becomes vanishingly small the lateral resolution improves by a factor of $\sqrt{2}$.

$$Confocal\,lateral\,resolution = \frac{r_{AIRY}}{\sqrt{2}} = \frac{0.86\lambda}{2NA} \tag{4.3}$$

The axial resolution of a confocal microscope is more difficult to obtain.

$$d_z(PL) = \frac{1.77\lambda}{(NA)^2} \tag{4.4}$$

$$d_z(RL) = FWHM = \frac{0.22\lambda}{n\sin^2\left(\frac{\theta}{2}\right)} \tag{4.5}$$

where θ is the same angle as in Fig. 4.3, and both equations assume zero-size pinholes. Equation 4.4 applies the Rayleigh criterion along the optical axis while equation 4.5 is derived from using paraxial (small angle) theory [11]. Both equations should be considered approximations, which in some cases will fail to predict the lateral resolution.

4.2 Photomultiplier

A photomultiplier tube (PMT) is characterized by its high sensitivity and fast response.

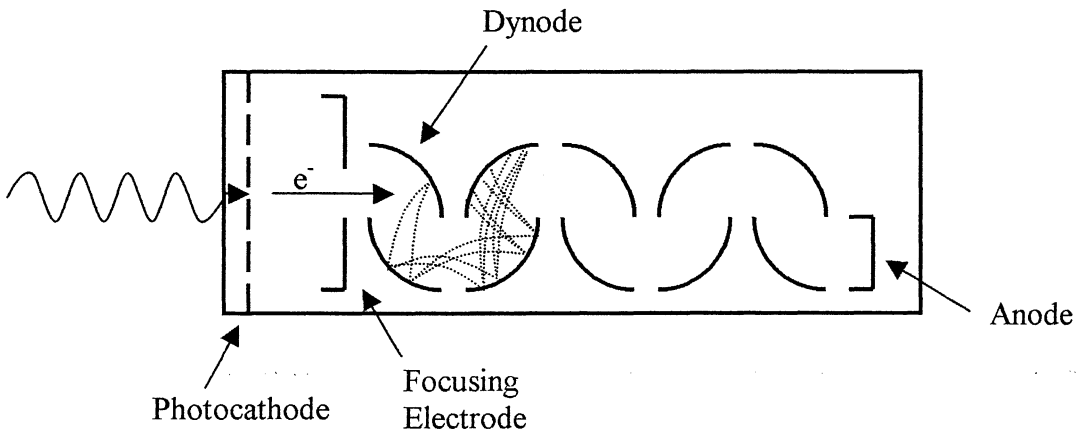

Figure 4.4 Schematic of a photomultiplier tube

Photons enter the PMT through a window. Different materials are used for the window, each of these have different spectral properties.

When light is absorbed by the photocathode, photoelectrons are emitted. The quantum efficiency is the number of photoelectrons emitted from the photocathode divided by the number of incident photons.

The emitted electrons are then accelerated, by an electric field, towards a dynode. For each electron hitting the dynode a number of secondary electrons are emitted. These secondary electrons are directed toward a secondary dynode. This goes on in many steps, each with a small gain. The electrons are finally collected by an anode, which provides a signal current.

The current amplification, which is the ratio between the anode output current and the photoelectric current from the photocathode, is in the order of 10^6. Ideally the current amplification factor of a photomultiplier tube having N dynodes and an average secondary emission ratio δ from each dynode is

$$G = \delta^N \tag{4.6}$$

The spectral response is expressed either by the radiant sensitivity or the quantum efficiency as a function of the wavelength. The radiant sensitivity (S) is the photoelectric current from the photocathode divided by the incident radiant power at a given wavelength. The relationship between the quantum efficiency and the radiant sensitivity at a given wavelength is

$$QE = \frac{S * 1.24 * 10^{-6}}{\lambda} \tag{4.7}$$

Where S is in A/W and λ is the wavelength.

Anode dark current

Even when there is no light incident on the photocathode there is a small current from the anode, called anode dark current. The major source of the anode dark current is thermionic emission of electrons from the photocathode. The reason for the thermionic emission is that the thermal energy, *kT*, is not neglible when compared to the work function of the photocathode. Photocathodes with a high sensitivity in the red to infrared, i.e. a low work function, show higher dark current.

The photocathode and the dynodes emit electrons even at room temperature. The major part of the dark current is due to thermionic emissions. Cooling the photomultiplier is a effective way to reduce thermionic emission.

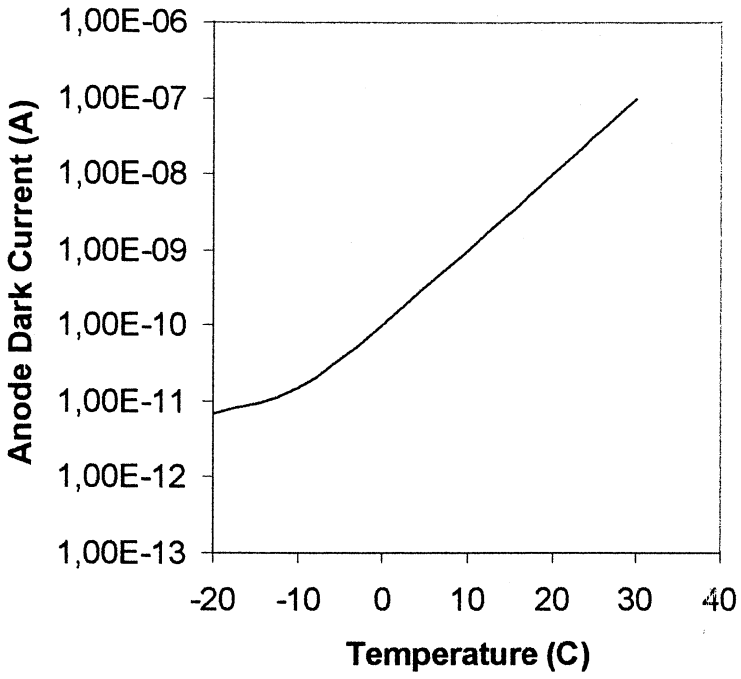

Figure 4.5 Temperature characteristics of dark current for a typical S20 multialkali photomultiplier.

The equivalent noise input (ENI) is the amount of light necessary to produce a signal-to-noise ratio of one from a photomultipler tube. The value of ENI is given by [12]

$$ENI = \frac{\sqrt{2 * q * i_{anode} * \Delta f}}{S} \tag{4.7}$$

Where q is the electronic charge, i_{anode} is the anode dark current, μ is the gain, Δf is the bandwith of the system and S is the anode radiant sensitivity.

5. Initial Raman Measurements

5.1 Introduction

The purpose of these measurements was to get a more practical knowledge of Raman spectroscopy and to identify compounds with Raman peaks suitable for testing Raman imaging.
With the method used for performing Raman imaging, as is shown in chapter 7, it was possible to use Raman peaks between 603 cm^{-1} and 828 cm^{-1}. The Raman spectra of several different compounds were measured. Suitable Raman peaks to test the method for Raman imaging were identified.

5.2 Experimental Set-up

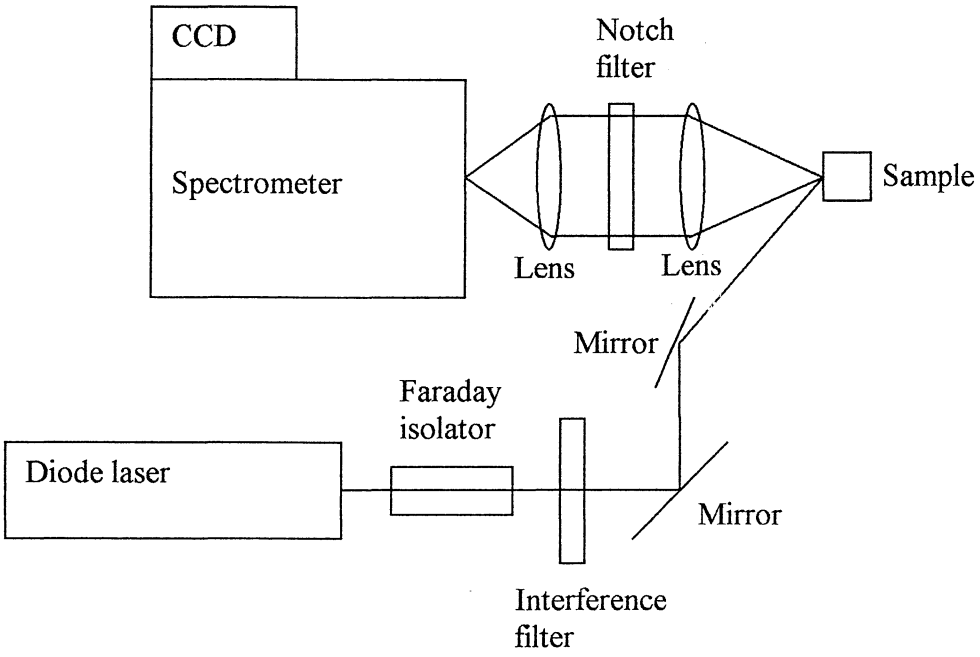

Figure 5.1 Experimental set-up for initial Raman measurements.

The set-up for the measurements is shown in Figure 5.1. As the light source a tuneable continuous wave diode laser (SDL-8630) was used. The laser is tuneable between 781-795 nm with the use of a motion controller (Motion Master 2000, Newport) that moves a grating inside the laser cavity. The laser has a maximum power of 0.5 W at 785 nm. The excitation was chosen in the NIR region, 784.5 nm, in order to reduce fluorescence from the samples. A Faraday isolator (Electro-Optical Technology Inc.) was inserted after the laser, to prevent any back reflections, from optical components, from getting coupled into the laser cavity and damaging the laser diode a Faraday isolator (Electro-Optical Technology Inc.) was inserted after the laser.

The laser light was not clean, but contained some unwanted light at slightly longer wavelengths than the laser line. To reduce this unwanted light a narrow band interference filter (784.5 nm Kaiser optical Inc.) was inserted.

The light was guided with the aid of two mirrors to the sample. Some of the scattered light from the sample was then collected with a collimating lens. The collimated beam of the scattered light passed through a notch filter (784.5 nm Kaiser Optical Systems, Inc.) to remove most of the Rayleigh scattered light. A lens then focused the light on the entrance slit of the spectrograph.

The spectrograph (Holospec f/1.8i, Kaiser Optical Systems, Inc.) uses a holographic grating to wavelength divide the light. As the detector a CCD camera (LN/CCD-1024 EHRB, Princeton Instruments, Inc.) was used. This CCD camera is back-illuminated and near-infrared-enhanced to increase the quantum efficiency. To reduce the thermal noise level the camera is cooled with liquid nitrogen.

The signals from the CCD camera were then processed in computer with a software program called Winspec. Winspec is able to remove the signals from high-energy cosmic particles from the spectra. This feature was used in the measurements.

To calibrate the set-up, a measurement on indene (C_9H_8) was done. The Raman spectra of indene have many peaks, which have been accurately measured. The peaks where identified and used for Raman calibration of the CCD (pixel-Raman shift).

A background spectra when no light entered the spectrograph was measured and then subtracted from the recorded spectra to correct for dark current counts in the CCD chip.

5.3 Results and discussion

The measurements were performed with the laser tuned to 784,5 nm and laser power of 150 mW.

The first measurement was done on Toluene (C_7H_8). This is liquid chemical with low fluorescence and relatively strong Raman signals. The acquisition time for the spectra was 10 s.

During the first measurements on toluene, some fluorescence background was present in the spectra. The conclusion was that the fluorescence emission originated from the glass cuvette in which the sample was kept during the measurements. By using a quartz cuvette instead the fluorescence background vanished.

Quartz glass (synthetic silica) is the preferable choice of optical material for Raman spectroscopy, as it does not fluoresce.

As is seen in the spectra Toluene has a very low fluorescence background and strong and easily identifiable Raman peaks. The strong Raman peak at 783 cm^{-1} can be used for Raman Imaging. This peak corresponds to a mono-substituted benzene ring vibration mode. The most prominent Raman peak at 1000 cm^{-1} arises from a symmetrical ring breathing mode.

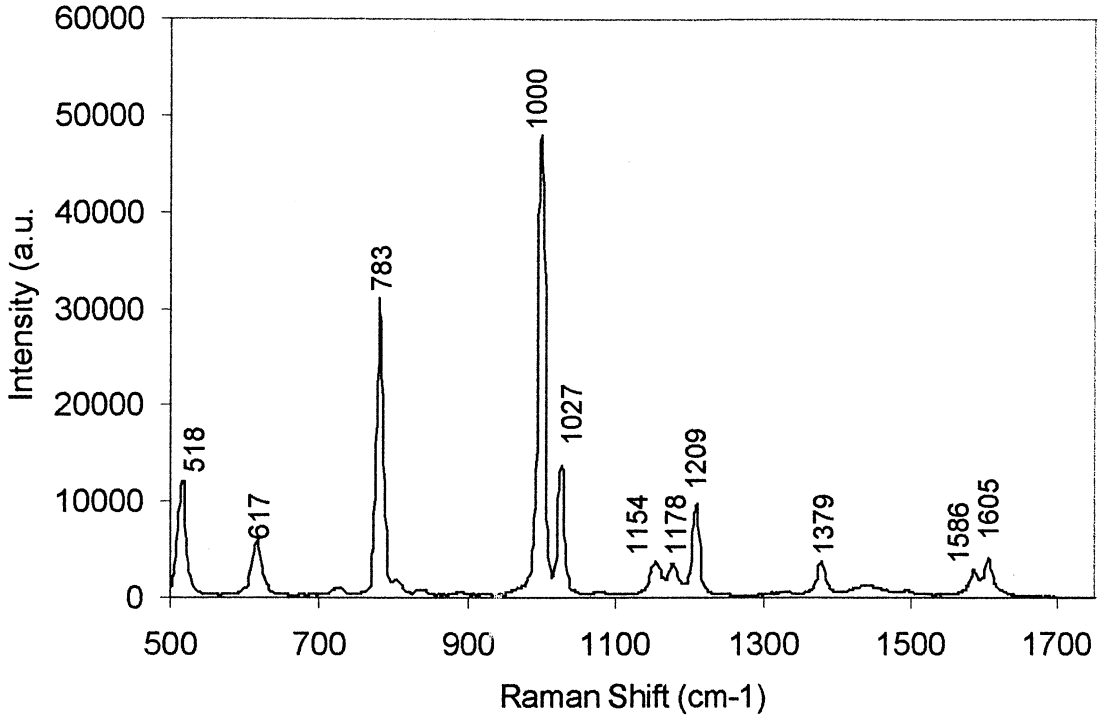

Figure 5.2. Raman spectra of Toluene (C_7H_8).

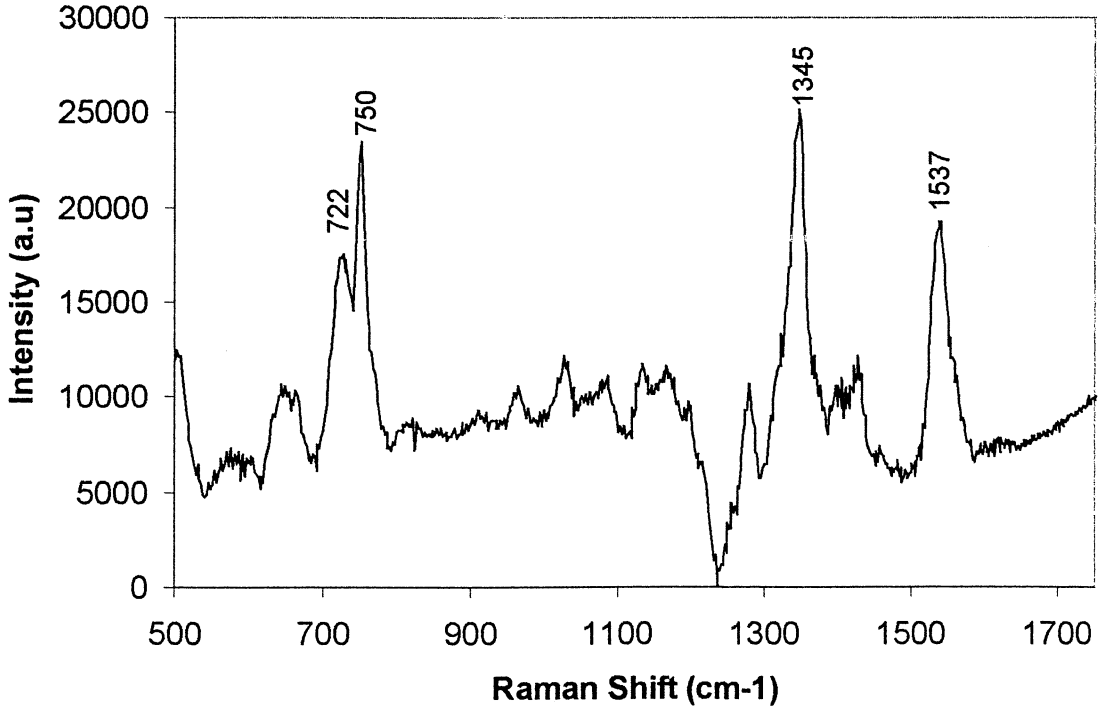

Figure 5.3 Raman spectra of Aluminium Phthalocyanine.

Measurements were also performed on Aluminium Phatalocyanine, see figure 5.3. The acquisition time of the spectra was 120s. Aluminium Phthalocyanine is used as a photosensitizer when performing Photodynamic therapy. The Raman spectra of Aluminium Phthalocyanine had a high fluorescence background. The fluorescence background was subtracted from the spectra by using a polynomial fit procedure, as is described in chapter 3.2.

The Raman peak at 750 cm^{-1} can be used for Raman imaging. This Raman peak arises from the phthalocyanine macrocycle ring stretching vibration mode.

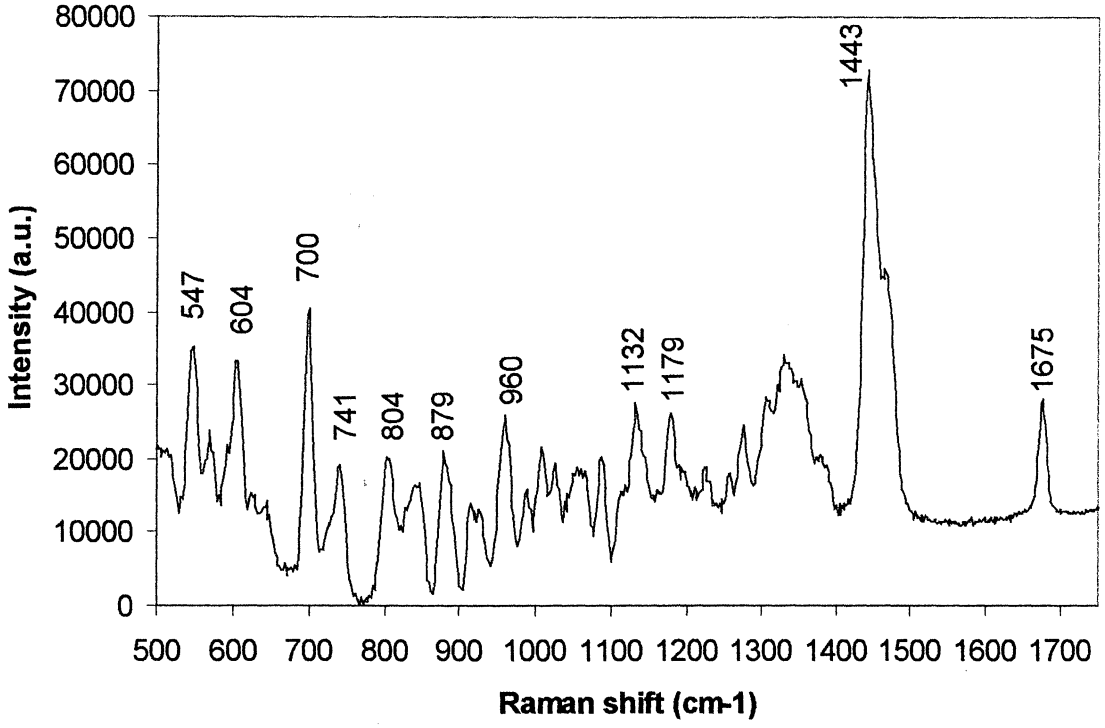

Figure 5.4 Raman spectra of cholesterol.

A measurement was also done on a pure tissue constituent in the form of Cholesterol ($C_{27}H_{46}O$). The acquisition time of the spectra was 120 s. A polynomial fit was done to reduce the fluorescence background. As is seen in the spectra cholesterol has many Raman peaks. This is due to the fact that cholesterol is a large molecule and therefore has many vibrational modes.

The Raman peak at 700 cm^{-1} is suitable for Raman imaging. This peak is from the sterol ring stretch vibration mode. The intense Raman peak at 1443 cm^{-1} is from the CH_2 bending mode.

6 Raman Microscopy

6.1 Introduction

The Raman Microscopy measurements were done in order to evaluate the set-up that would be used for Raman Imaging. The set-up for Raman microscopy was very similar to the one used for Raman imaging. The major difference is how the scattered light from the sample is collected. The set-up for Raman imaging uses confocal microscopy with the optics in the scanhead and a photomultiplier as detector, but the set-up for Raman Microscopy uses normal microscopy and a CCD as detector.

6.2 Experimental setup

The experimental set-up that was used for Raman microscopy is shown in Figure 7.1.

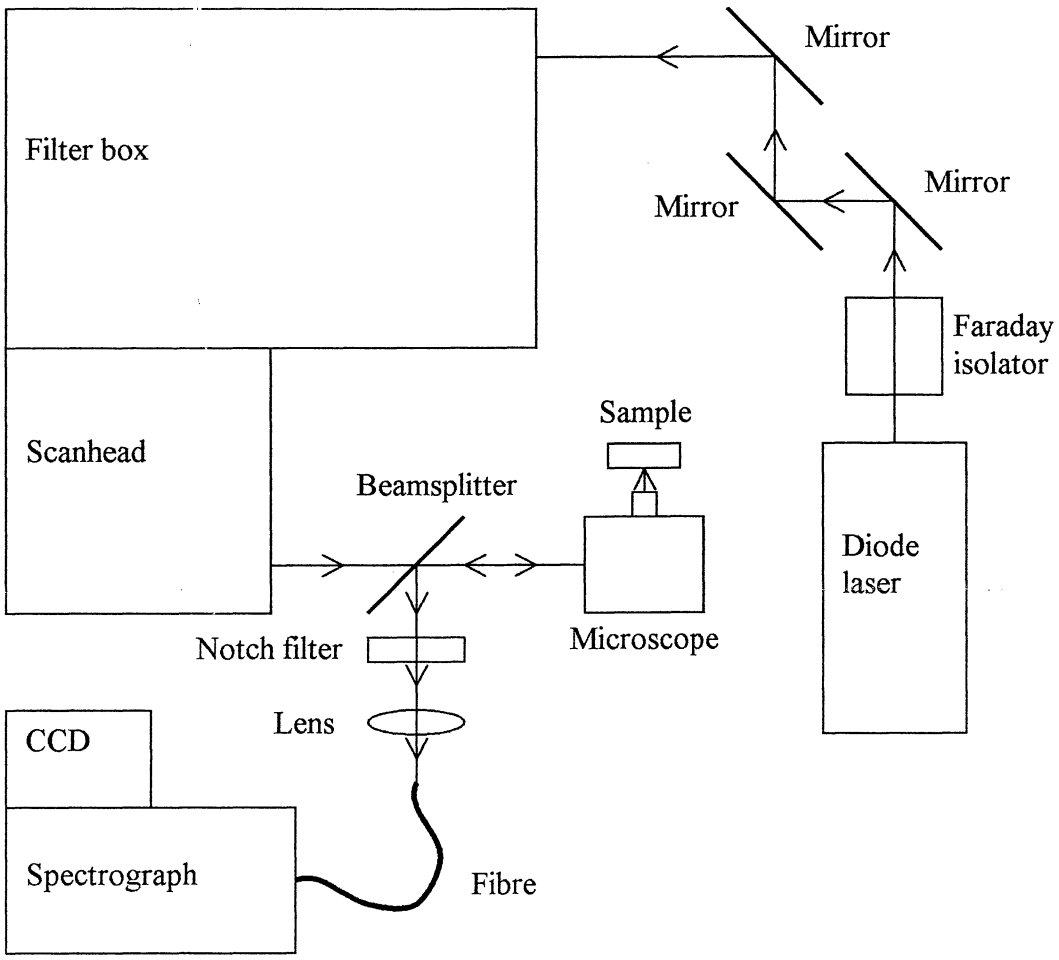

Figure 6.1. Set-up for Raman microscopy.

The laser used was the SDL-8630 tuneable continuous wave diode laser. This laser has a maximum power of 0.5 W at 785 nm. A Faraday isolator was placed directly after the laser to

prevent any back reflections from the optical components to damage the laser diode. Through a set of three mirrors the light was guided into the laser scanning confocal microscope (MRC 1024, Bio Rad Microscopy Division).

The light from the laser contained some emission at slightly longer wavelengths than the laser line, which could interfere with the measurements. This unwanted light was reduced by placing a bandpass filter (790bp-w, Chroma Technology Corp.) in the scanhead.

As the laser light left the scan head it passed through a 50/50 beam splitter and into the microscope (Nikon Diaphot 300) where it was focused onto the sample by the microscope objective (Plan 40/0.70 Nikon). The scattered light was collected by the same microscope objective and led back to the beam splitter. The beam splitter reflected the light onto a notch filter (Kaiser Optical Inc.). This notch filter was used to reduce the Rayleigh-scattered light from the sample. The light was then focused by a lens into a fibre (600 μm Anhydroguide) and led to the spectrograph (Holospec f/1.8i, Kaiser Optical Systems Inc.).

The wavelength divided light was then detected by an CCD camera (LN/CCD-1024 EHRB Princeton Instruments Inc.). This CCD was back-illuminated and near infrared enhanced to increase the quantum efficiency and also nitrogen cooled to reduce the noise. Winspec was then used to process the signals from the CCD. The feature to remove the effects of cosmic particles in the spectra was enabled.

When the system was used in the scanning mode the focused light at the fibre moved, so the beam had to be parked in one place on the sample.

Raman calibration was performed by a measurement on indene and four of the Raman peaks where identified and used for calibration.

6.3 Results and discussion

The Raman spectra were measured for different samples. The power out from the laser was 282 mW, of this 210 mW was left after the Faraday isolator. Of this 23mW was left when the light exited the scanhead. The amount actually reaching the sample could not be measured because of the very divergent beam after the microscope objective.

Toulene (C_7H_8) is a liquid chemical. It shows relatively strong Raman signals and low fluorescence background. The total acquisition time for the spectra was 300 s. If you compare the spectra with figure 5.2, it is evident that we now have a fluorescence background. This background is probably from fluorescence from the fibre and optical components made of glass that are present in the experimental set-up.

Rhodamine 6G ($C_{28}H_{31}N_2O_3Cl$) is a laser dye. When used in a dye laser, it is tuneable from 560nm to 650 nm. Rhodamine 6G can be characterized as a highly fluorescent substance. The acquisition time for the spectra was 300s. Rhodamine 6G has a Raman peak at 610 cm-^{1} and one at 767 cm^{-1} that is suitable for Raman imaging.

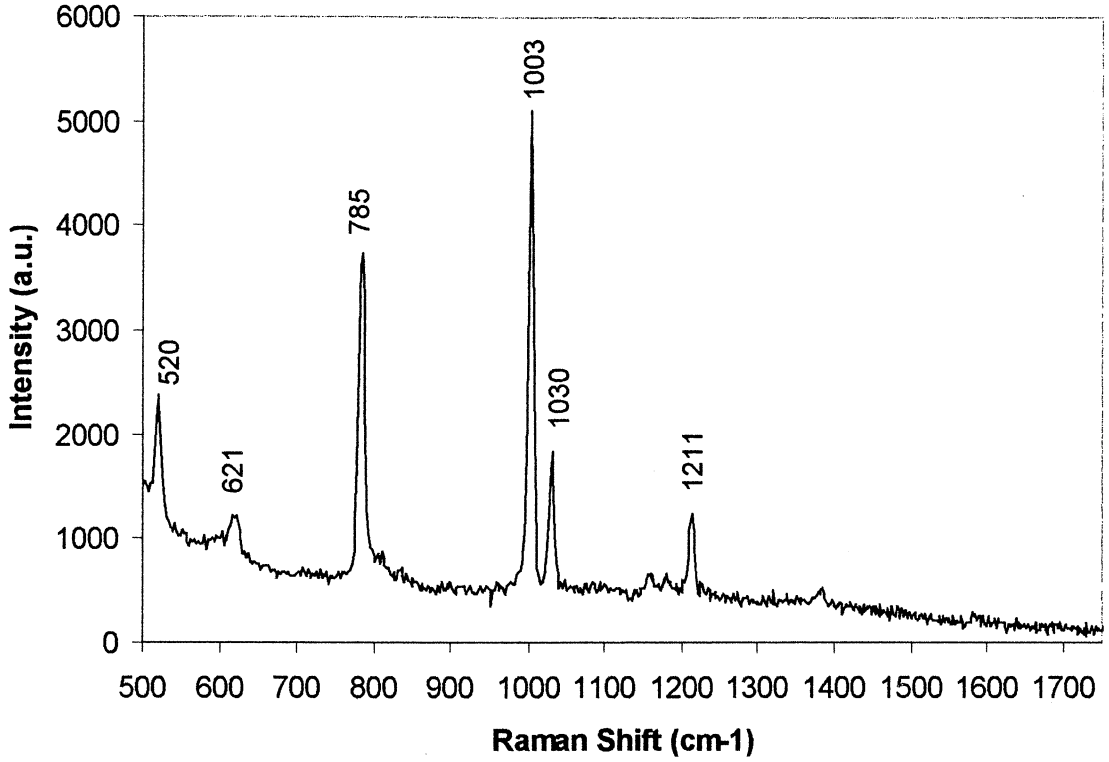

Figure 6.2. Raman spectra of Toluene

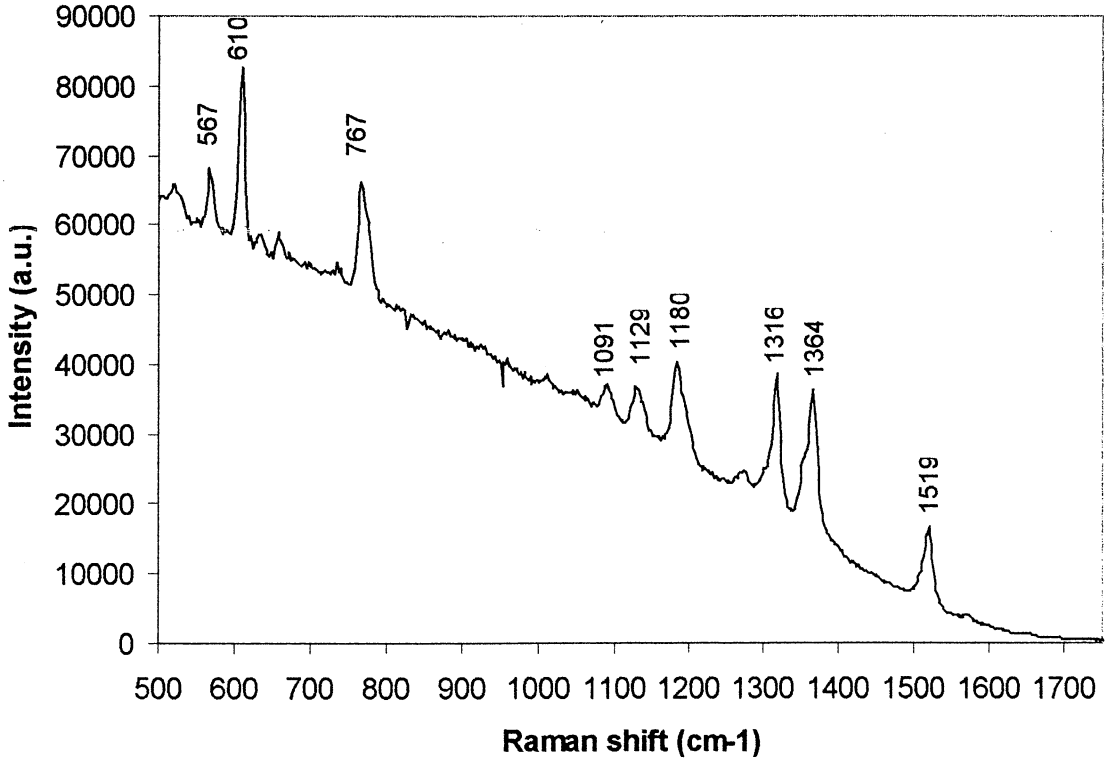

Figure 6.3. Raman spectra of Rhodamine 6G

With the measurements it is shown that it is possible to do Raman microscopy, even if the Raman signals are very weak. The reason for this is that the intensity of the excitation light at the sample is low and that a lot of the scattered light from the sample is lost on its way back to the detector.

The biggest problem with the set-up was the losses of light. Of 210 mW of power that was present after the Faraday isolator, only 23 mW was left after the scanhead. The major part of these losses occurred in the scanhead. Because the scanhead cannot be opened it was impossible to tell which parts where responsible. The poor performance of the scanhead in the near-infrared region has been noted by others [13].

For the choice of beamsplitter it would have been preferable to have a dichroic mirror that would transmit the laser light at 785 nm and reflect the scattered light with a longer wavelength. No dichroic mirror with these properties where available, instead a 50/50 beamsplitter where used. This beamsplitter transmits 50% and reflects 50% of the light. This means that half of the excitation light is lost, and also half of the scattered light on its way to the detector.

It was also noted that the spot size of the laser beam was larger than the entrance aperture of the microscope objective, so additional light was lost here.

7. Confocal Raman Imaging

7.1 Introduction

The method used to perform Raman Imaging is a series-imaging method with point illumination using a laser scanning confocal microscope. The Raman signal from the molecular species to be imaged is spectrally filtered out with a narrow bandpass filter.

7.2 Experimental set-up

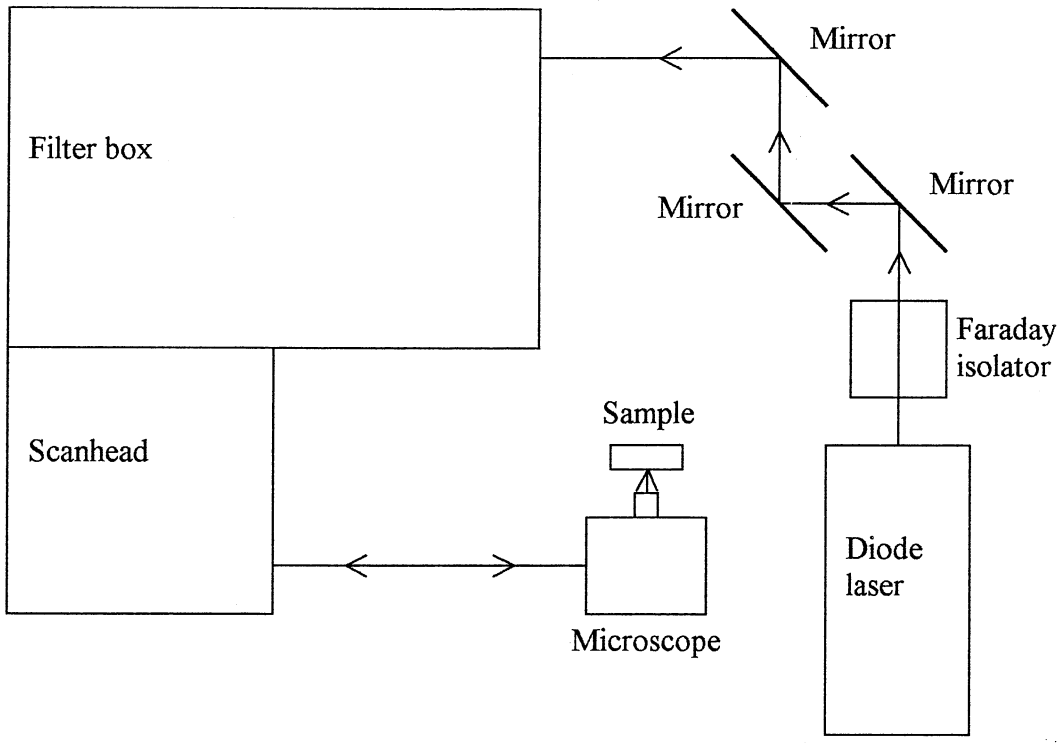

Figure 7.1. Set-up for Confocal Raman Imaging.

The light source was the SDL-8630 continous wave diode laser. This laser is tuneable in an interval between 781-795 nm, by using a motion controller (Motion Master 2000, Newport) that moves a grating inside the laser cavity. To prevent back reflections from damaging the laser diode, a Farraday isolator was used directly after the laser. The laser beam was then guided with a set of 3 mirrors into the near infrared path of the filter box and then into the scan head of the laser scanning confocal microsope (MRC1024, Bio Rad Microscopy Division).

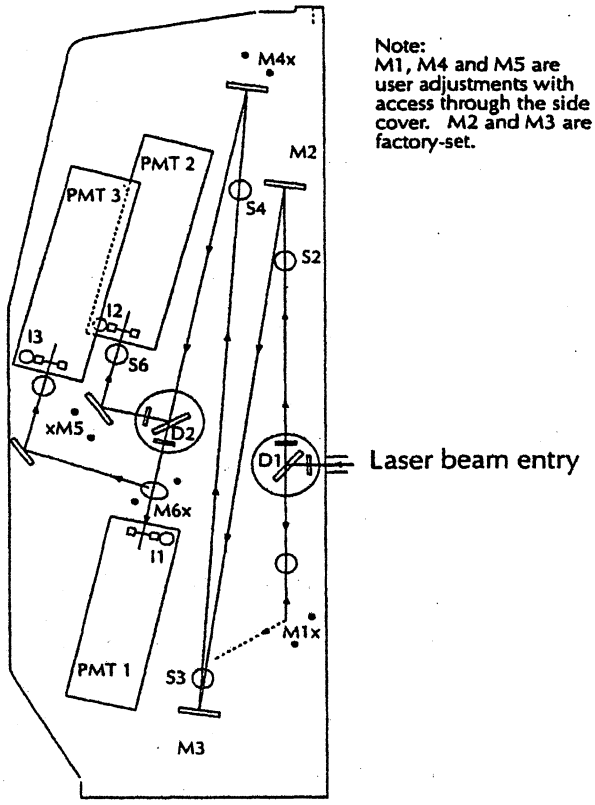

Figure 7.2 Scanhead of the laser scanning confocal microscope [1].

A dichroic mirror (810 dc Chroma Technology Corp.) and a bandpass filter (790bp-w Chroma technology Corp.) were inserted in the first filter block (D1 in figure 7.2). The band pass filter reduced the unwanted light present in the beam apart from the laser line. The dichroic mirror reflected the laser beam to the scanning mirrors. The laser light then entered the microscope and was focused onto the sample by the microscope objective. The same objective collected the scattered light from the sample and this light then enters the scanhead. The dichroic mirror, in the filterblock transmitted the elastically scattered light from the sample while reflecting the Rayleigh scattered light. A narrow-banded interference filter (835bp1 Chroma Technology Corp.) was inserted into the second filter block (D2 in figure 7.2). This filter reduces all light apart from 835+-1 nm. M6x is a dichroic mirror which reflects wavelengths above 640 nm to PMT3. PMT3 was used for detection.

The transmittance for the 790bp-w, 810 dc and 835bp1 filters is shown in the appendix.

7.4 Method for Raman Imaging

The following method was used with the experimental set-up to conduct Raman imaging. The laser was tuned to a wavelength so that the 835bp1 filter would match the desired Raman peak for the molecular species that would be imaged. The laser wavelength was given by

$$\lambda_{laser} = \frac{1}{\Delta\bar{\nu} + \frac{1}{\lambda_{filter}}} \qquad (7.1)$$

Where $\Delta\bar{\nu}$ is the desired Raman shift and λ_{filter}=835nm.

The laser in tuneable between 781 and 795 nm, which means that Raman shifts between 603 and 828 cm^{-1} is reachable with the bandpass filter.

An image was acquired with the laser set at this wavelength. As the image would contain some background from fluorescence emission, it was necessary to correct the image for this. By tuning the laser slightly the bandpass filter would come beside the Raman peak and a background image could be acquired. The background image was then subtracted from the initial image, which resulted in a Raman image.

7.5 Results and discussion

Measurements were done on the 767 cm^{-1} Raman peak of Rhodamine 6G, 700 cm^{-1} Raman peak of Cholesterol, the 750 cm^{-1} Raman Peak of Aluminium Phatalocyanine and the 783 cm^{-1} Raman peak of Toluene.

Raman imaging was not possible with this equipment due to the noise. The conclusion is that the signal-to-noise ratio for the experimental set-up is to low. The following reason can explain this.

Reasons for too low signal.

* Much of the light from the laser is lost on its way to the sample. A major part of these losses occur in the scanhead. These losses are explained in chapter 6.

* Because a lot of the laser light is lost in the scanhead on its way to the sample, it is probable that a lot of the scattered light from the sample is lost on its way to detector. Because the scanhead cold not be opened it was impossible to tell which parts where responsible. The 810dc has a transmittance of 94% at 835 nm and the 835bp1 has a peak transmittance of 75% at 835 nm.

* The collection efficiency of confocal microscopes is low when compared to a normal microscope. This is due to the fact that intentional rejection of light by the confocal aperture is done to get resolution in depth.

* The PMT has very low quantum efficiency at 835 nm. The quantum efficiency of the detector is shown in figure 7.3.

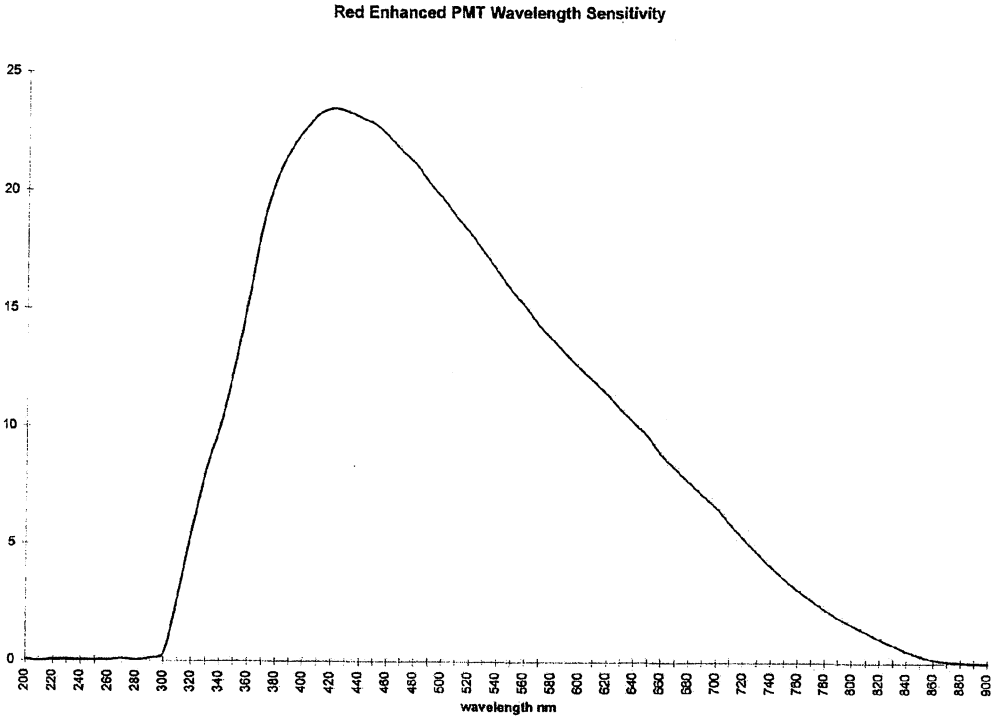

Fig 7.3 Quantum efficiency of photomultiplier

At 835 nm the quantum efficiency of the photomultiplier tube is 0.6%. This means that the radiant sensitivity is

$$S_{cathode} = \frac{QE * \lambda}{1.24 * 10^{-6}} = \frac{0.006 * 835 * 10^{-9}}{1.24 * 10^{-6}} = 4 * 10^{-3} A/W \qquad (7.2)$$

Reasons for too much noise

* The PMT is not cooled, and because it has a relative high sensitivity in the red/near-infra-red the photocathode has a low workfunction. Bio-Rad was reluctant to specify the type or supplier of the photomultiplier tube, but it is probably a multialkali S20 type. The photomultiplier tube is mounted enclosed in the scanhead. The temperature inside the scanhead is somewhere above room temperature. At 30C a S20 PMT has a typical anode dark current of around 100nA.

* To get an image you measure a large number of pixels. This means that the collection time for the signal from each pixel is not very long. A total acquisition time for the image (256*256 pixels) of ten minutes correspond to a collection time for the signal from a pixel of

$$t_{pixel} = \frac{600}{256^2} = 0{,}0092\,\mathrm{s} \qquad (7.3)$$

The noise equivalent power, expressed in Eq. (3.2), for the photomultiplier tube with these values is estimated to be

$$NEP = \frac{\sqrt{2 * q * ldb * \mu * \Delta f}}{S_{cathode} * G} \approx 10^{-12} W \qquad (7.4)$$

Other solutions

To be able to do Raman Imaging you have to increase the signal-to-noise ratio. Increasing the signal and/or decreasing the noise can accomplish this. One solution, which will achieve both an increase in the signal and a decrease in the noise, is to use an external detector.

Bio Rad has supplied a mounting for an external detector to be placed between the scanhead and the microscope. Similar to the set-up used for Raman microscopy, this mounting uses a dichroic mirror to reflect the scattered light from the sample to a detector.

With this set-up it is possible to select a photocathode with more radiant sensitivity in the near-infrared. For example GaAs, which has a radiant sensitivity of around 80mA/W at 835 nm. You are also able to cool the photomultiplier tube to reduce dark current. Which such a photomultiplier you are able to get a noise equivalent power, expressed in Eq. (3.2), which can be estimated to be

$$NEP = \frac{\sqrt{2 * q * ldb * \mu * \Delta f}}{S_{cathode} * G} \approx 10^{-15} W \qquad (7.5)$$

When you use an external detector, you also gain a lot of scattered light when compared to using the internal photomultiplier tubes in the scanhead. There are two major reasons for this.

When you use an external detector the set-up is not confocal, i.e. you do not reject out of focus light, and the collection efficiency is considerably higher compared to using the photomultiplier tubes in the scanhead.

Scattered light is also gained, as you do not use the optics in the scanhead, which is proven to be lossy for near-infrared light, to collect the scattered light from the sample.

8. Acknowledgements

I would like to thank my supervisor, Stefan Andersson-Engels, for his his guidance in making this thesis possible. I would also like to express my sincere gratitude to Sara Pålsson for introducing me to the field of Raman spectroscopy, and to Per Peterson for his help with understanding the Confocal Microscope.

9. References

1. S. Svanberg, "Atomic and Molecular Spectroscopy", 2nd ed., Springer-Verlag, 1992

2. T. Tahara and H. O. Hamaguchi, "Picosecond Raman Spectroscopy Using a Streak Camera", Applied Spectroscopy, 47, 391-398, (1993)

3. P.-E. Bengtsson, M. Aldén, S. Kröll, and D. Nilsson, "Vibrational CARS Thermometry in Sooty Flames: Quantitative Evaluation of C_2 Absorption Interference", Combustion and Flame, 82, 199-210, (1990)

4. N. M. Sijtsema, J. J. Duindam, G. J. Puppels, C. Otto and J. Greve, "Imaging with Extrinsic Raman Labels", Applied Spectroscopy, 50, 545-551 (1996).

5. G. J. Puppels, M. Grond and J. Greve, "Direct Imaging Raman Microscope Based on Tunable Wavelength Excitation and Narrow-Band Emission Detection", Applied Spectroscopy, 47, 1256-1267 (1993).

6. G. Turrell and J. Corset, "Raman Microscopy", Academic Press (1996)

7. C. J. H. Brenan and I. W. Hunter "Confocal Image Properties of a Confocal Laser Visible Light FT-Raman Microscope", Applied Spectroscopy, 49, 971-976 (1995).

8. C. A. Drumm and M. D. Morris "Microscopic Line-Imaging with Principal Component Analysis", Applied Spectroscopy, 49, 1331-1337 (1995).

9. T. L. Freeman, S. E. Cope, M. R. Stringer, J. E. Cruse-Sawyer, S. B. Brown and D. N. Batchelder, "Mapping the Distribution of Zinc Phthalocyanine Derivatives in EAhy 926 Cells using Raman Microscopy", Progress in Biomedical Optics, 168-176 (1997).

10. Bio-Rad Microscopy division, "MRC-1024 Laser Scanning Confocal Imaging System: User operating Manual", 1996

11. J. B. Pawley, "Handbook of Biological Confocal Microscopy", 2nd ed., Plenum, 1995

12. Hamamatsu Photonics K.K., "Photomultiplier tubes", 1998

13. P. Peterson, "Two-photon excited laser scanning confocal microscopy", Diploma Paper, Lund Reports on Atomic Physics, 1997

10. Appendix

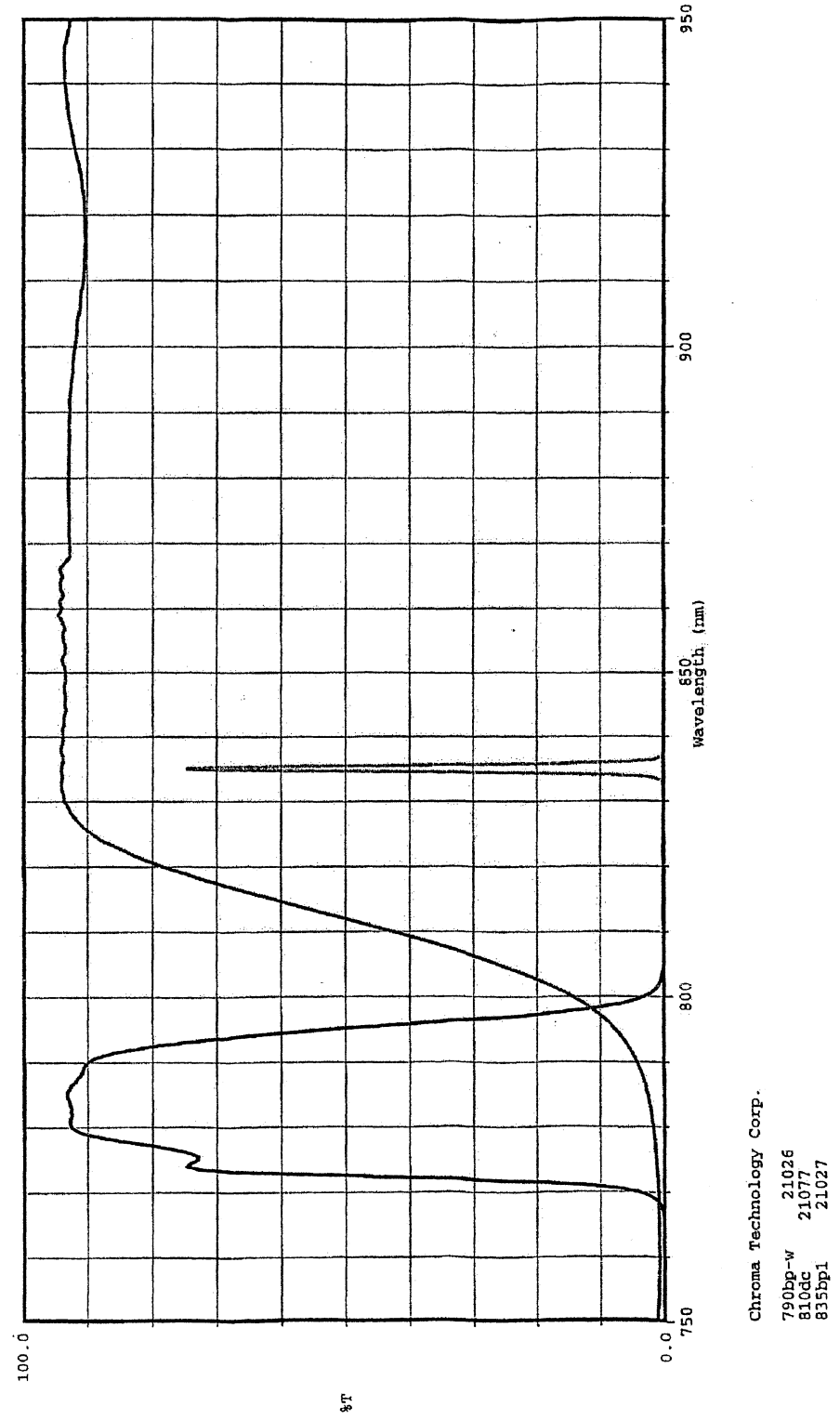

Figure 9.1 Transmittance of 790bp-w, 810 dc and 835bp1.